Array antenna diagnostics with the 3D reconstruction algorithm

Cappellin, Cecilia; Meincke, Peter; Pivnenko, Sergey; Jørgensen, Erik

Published in:
Proceedings of the 34th Annual Symposium of the Antenna Measurement Techniques Association

Publication date:
2012

Document Version
Publisher's PDF, also known as Version of record

ARRAY ANTENNA DIAGNOSTICS WITH THE 3D RECONSTRUCTION ALGORITHM

Cecilia Cappellin[1], Peter Meincke[1], Sergey Pivnenko[2], Erik Jørgensen[1]

[1]TICRA, Læderstræde 34, DK-1201 Copenhagen, Denmark
[2]DTU Elektro, Technical University of Denmark, Ørsteds Plads, Building 348, 2800 Kgs. Lyngby, Denmark

ABSTRACT

The 3D reconstruction algorithm is applied to a slotted waveguide array measured at the DTU-ESA Spherical Near-Field Antenna Test Facility. One slot of the array is covered by conductive tape and an error is present in the array excitation. Results show the accuracy obtainable by the 3D reconstruction algorithm. Considerations on the measurement sampling, the obtainable spatial resolution, and the possibility of taking full advantage of the reconstruction geometry are provided.

Keywords: Array, Diagnostics, Resolution, Spherical Wave Expansion, Inverse Method of Moments

1. Introduction

Accurate and general antenna diagnostics techniques to identify, from the radiated measured field, the electrical and mechanical errors affecting the antenna under test are of high importance for the antenna measurements community. Microwave holography, based on the well-established relation between the antenna far-field and the visible region of the plane wave spectrum [1], has been widely used for this purpose. The algorithm is general, simple and computationally very fast but has a limit in the spatial resolution of the computed extreme near-field, since the invisible region of the plane wave spectrum is always neglected. The technique presented in [2] allows the reconstruction of part of the invisible region of the plane wave spectrum, thus providing higher resolution in the computed extreme near-field, but shows some limitation when dealing with large antennas and typical measurement noise.

To overcome these limits, a new class of antenna diagnostics algorithm has been introduced in the last decade. These new methods are based on the discretization of integral equations, see [3]-[9], which are derived by placing unknown equivalent electric and magnetic currents on a surface conformal to the antenna and requiring that the currents radiate the measured field outside the surface and zero field inside the surface. A discrete set of equations are obtained by using a standard Method of Moments discretization, e.g., RWG functions on flat triangular facets [5], or higher-order basis functions on curved surfaces [8]. The latter choice has shown to provide better accuracy and lower memory requirements [8]. Although more demanding in terms of memory usage and computation time as compared to microwave holography, these new methods allow reconstructing the field on an arbitrary 3D surface enclosing the antenna. The 3D reconstruction algorithm developed by TICRA in [8]-[9] is implemented in the commercial software DIATOOL.

The identification of array element failure is of particular interest for antenna diagnostics, and mainly documented in the literature through experimental results, see for example [13]. Diagnostics of array failure, however, focuses often on results achieved by microwave holography, which is intrinsically limited in accuracy. Though noticeable improvements were recently achieved by [14], all proposed techniques assume the knowledge of the array element factor, either from a dedicated measurement or a software simulation. To our knowledge, the enhanced capabilities of the 3D reconstruction algorithm on array diagnostics have not been studied in detail yet.

The purpose of this work is thus to study the accuracy achievable by the 3D reconstruction algorithm when dealing with a slotted waveguide array of which measured data are available. Considerations on the measurement sampling, the obtainable spatial resolution, and the possibility of taking full advantage of the reconstruction geometry will be provided.

The paper is organized as follows: Section 2 summarizes the main features of the 3D reconstruction algorithm implemented in DIATOOL, Section 3 describes the investigations performed on a slotted waveguide array measured at the DTU-ESA Spherical Near-Field Facility, while conclusions are drawn in Section 4.

2. The 3D Reconstruction Algorithm

The higher-order inverse Method of Moments algorithm, [8]-[9], was introduced as an extension of previously available integral-equation based reconstruction techniques. The method computes the tangential electric and magnetic fields $\bar{E}, \bar{H}$ on the reconstruction surface S enclosing an antenna, based on the field measured at discrete points outside the surface.

The tangential fields on the reconstruction surface *S* are obtained by the equivalent electric and magnetic surface current densities $\bar{J}s$ and $\bar{M}s$ according to

$$\bar{J}s = \hat{n} \times \bar{H}, \tag{1}$$

$$\bar{M}s = -\hat{n} \times \bar{E} \tag{2}$$

with $\hat{n}$ being the outward normal unit vector. These equivalent currents correspond to Love's equivalence principle, since they produce zero field inside *S*, and are found by solving the so-called data equation, which relates the measured data and the unknown surface current densities,

$$\bar{E}^{meas} = -\eta_0 L\bar{J}s + K\bar{M}s, \tag{3}$$

where η_0 is the free space impedance and L and K are integral operators defined in [8]. The a priori information that the fields radiated by the surface current densities must be zero inside *S* is then enforced as a boundary condition equation [6] and the correct set of equivalent surface current densities is finally found. The surface of reconstruction is discretized using curvilinear patches of up to fourth order. The electric and magnetic surface currents densities on each patch are expanded in higher order Legendre basis functions

$$\bar{X} = \sum_{m=0}^{M^u} \sum_{n=0}^{M^v-1} a_{mn}^u \bar{B}_{mn}^u + \sum_{m=0}^{M^v} \sum_{n=0}^{M^u-1} a_{mn}^v \bar{B}_{mn}^v, \tag{4}$$

where $\bar{X} = [\bar{J}s, \bar{M}s]$, a_{mn}^u and a_{mn}^v are unknown coefficients, M^u and M^v are the expansion orders along the *u*- and *v*- directions, and $\bar{B}_{mn}^u$ and $\bar{B}_{mn}^v$ are the *u*- and *v*-directed higher-order Legendre basis functions defined in [8] and [10]. The current expansion of Eq. (4) is then inserted in the data equation of Eq. (3) and the above mentioned boundary condition equation. These coupled equations are finally solved by the iterative solution scheme described in [9], which allows one to achieve an accurate solution by balancing the effects of noise with the requirement of achieving Love's currents. The inverse Method of Moments algorithm in DIATOOL differs from other similar methods [4]-[6] in three important aspects. First, the geometry and unknown currents are represented by smooth polynomial functions. Second, the testing of the boundary condition operator is performed *on* the actual surface of reconstruction. Third, a new regularization scheme is employed, in which the data equation and the boundary condition are treated separately. These differences result in improved efficiency, enhanced accuracy, and better resolution properties.

3. Slotted Waveguide Array

The 3D reconstruction was applied to a 6 by 7 slotted waveguide array of dimensions 30 cm by 27 cm working at 5.25 GHz, with different row excitations and a conductive tape covering one slot, as shown in Figure 1.

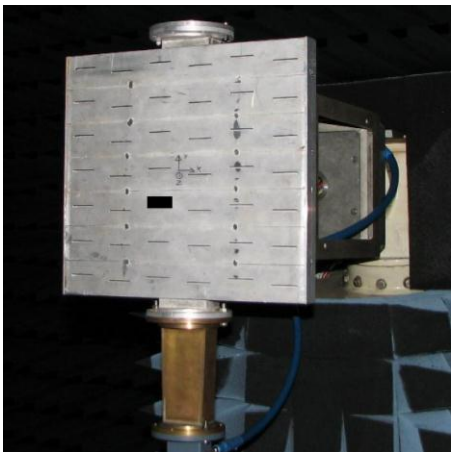

Figure 1 – The 6 by 7 slotted waveguide array in the DTU-ESA Spherical Near-Field Antenna Test Facility.

The antenna was measured at the DTU-ESA Spherical Near-Field Antenna Test Facility on a full sphere, with sampling in theta and phi equal to 2° and 4.5° respectively, and a SNR of 70 dB. The measurement coordinate system is shown in Figure 1: the origin coincides with the geometrical center of the array, the *x*-axis is horizontal, the *y*-axis is vertical and the *z*-axis points out of the paper. The distance between slots is 0.67 λ, with λ being the wavelength, along the vertical *y*-axis, and 0.85 λ along the horizontal *x*-axis. Since the product kr_o, where *k* is the wavenumber and r_o the radius of the antenna minimum sphere, is equal to 21, one finds that the Spherical Wave Expansion (SWE) of the field radiated by the antenna can be truncated to *N*=31, according to [12]

$$N = kr_o + \max\ 10, 3.6\sqrt[3]{kr_o}\ . \tag{5}$$

Once the maximum *N* is found, the sampling on the measurement sphere must at least be equal to

$$\Delta\theta = \Delta\varphi = \frac{180^\circ}{N} \tag{6}$$

which becomes $\Delta\theta$=$\Delta\varphi$=5.8° for *N*=31. Consequently, the field measured at the DTU-ESA Facility has an oversampling factor of 2.9 in theta and 1.3 in phi,

relative to the value of 5.8, and provides 7280 field samples distributed over the measurement sphere.

The number of measured field samples sets an upper limit for the maximum number of unknowns that the 3D reconstruction algorithm can solve. In DIATOOL the maximum number of unknowns is approximately equal to twice the number of measurement samples, in the present case around 14500. The number of unknowns depends on the number of patches used to mesh the closed surface, on which the currents are reconstructed. Moreover, it depends on the accuracy of the polynomial expansion used to represent the unknown currents. The polynomial expansion order is automatically adapted to the electrical size of each patch, leading to the so-called "normal" accuracy. It can, however, be increased by an order at a time, by using "enhanced", "high" or "extreme" accuracy, if necessary. The "normal" and "enhanced" settings are in general sufficient when dealing with measured data with 70 dB SNR. The maximum dimension of the patches used in the mesh of the reconstruction is 2 λ. Though it is recommended to use as large patches as possible, in order to limit the memory usage and the computation time, it was found that the possibility of decreasing the patch dimension plays an important role in the reconstruction capabilities, as it will be discussed in the next paragraph.
The reconstruction surface was a box enclosing the slotted waveguide array of Figure 1, with sizes 32 cm by 28 cm by 2 cm, with the top face coinciding with the array aperture. First, the maximum dimension of the patches was set to the default value of 2 λ and the "enhanced" accuracy was chosen. This gave rise to 30 patches over the reconstruction box and 4536 unknowns. The amplitude in dB of the *y*-component of the reconstructed tangential electric field on the top face of the box is shown in Figure 2, together with the used patches and the location of the covered slot. It is seen that it possible to distinguish the 6 by 7 slots and that the radiation on the covered slot location looks different with respect to the rest of the aperture.

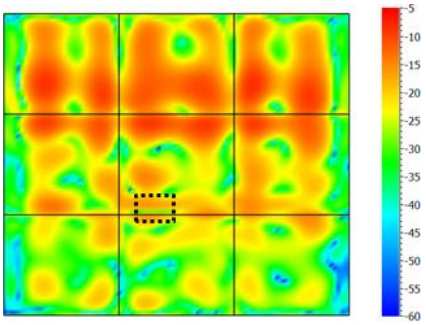

Figure 2 – Amplitude of the *y*-component of the tangential electric field from the 3D reconstruction, with patch size of 2 λ and enhanced accuracy.

The length of the patches was then reduced to 0.8 λ, which almost coincided with the spacing of the slots along the horizontal axis, and gave rise to 142 patches over the reconstruction box. By keeping the "enhanced" accuracy the number of unknowns became 8608. The result of the reconstruction is shown in Figure 3. It is seen that the individual slots are better resolved when compared to Figure 2, both in the columns and rows, and that the covered slot is now clearly identified. Moreover, it can be observed that the slot rows 2 and 3 are strongly excited whereas rows 6 and 7 are very weak. This is in contradiction with the expected array excitation, which postulates a symmetric excitation relative to row 4, with row 4 being the one excited the most. This indicates that an error is present in the array feeding network. The result given by the traditional microwave holography on a plane of 32 cm by 28 cm located on the array aperture is shown in Figure 4. While the picture shows areas of high and low excitation similar to what is shown in Figure 2 and Figure 3, it is evident that the individual slots cannot be resolved, and that the resolution of the 3D reconstruction is far higher than the one provided by microwave holography.

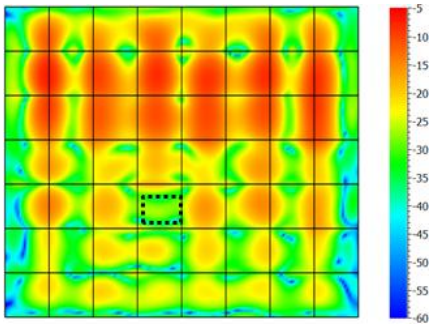

Figure 3 - Amplitude of the *y*-component of the tangential electric field from the 3D reconstruction, with patch size of 0.8 λ and enhanced accuracy.

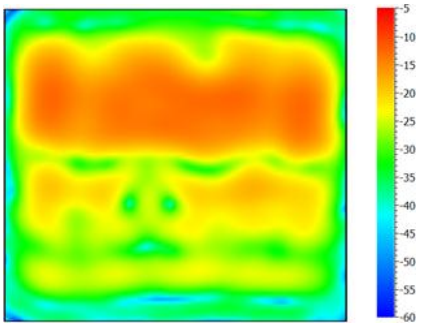

Figure 4 - Amplitude of the *y*-component of the tangential electric field from traditional microwave holography.

3.1) Effect of Truncated Measurement Sphere and Sampling Density

It was then decided to study if truncating the measurement sphere and decreasing the number of measured samples had an effect on the reconstructed field.

To study the measurement truncation effect, the measured sphere was truncated to 80˚, while keeping the original sampling of 2˚ in theta and 4.5˚ in phi. This gave rise to 3280 measured samples. By zero padding the remaining part of the sphere the available samples became 5315 and allowed to reconstruct the field with "enhanced" accuracy and 0.8 λ for the patch size. The result is shown in Figure 5: the reconstructed field is less accurate than that presented in Figure 3, i.e. the slots start overlapping, but still better than Figure 4 since the slots can still roughly be identified. The truncated sphere was then reduced to 70˚ and 60˚ respectively, always zero padding the remaining part of the sphere. The reconstruction was performed again with 0.8 λ and with "enhanced" accuracy and it was observed that with 60˚, see Figure 6, slots could no longer be resolved and the result looked similar to the microwave holography picture of Figure 4. By inspecting the measured field pattern, it was found that for theta belonging to [-80˚:80˚] and to [-70˚:70˚] the lowest value of the co-polar component was -35 dB from the peak, while for theta belonging to [-60˚:60˚] it became equal to -30 dB.

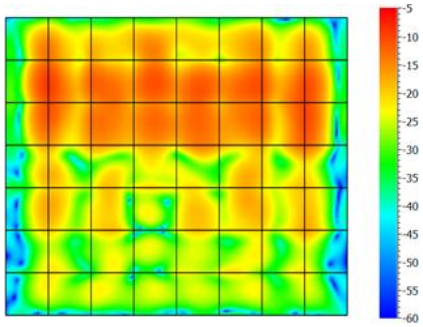

Figure 5 - Amplitude of the *y*-component of the tangential electric field from the 3D reconstruction, with patch size of 0.8 λ, enhanced accuracy and a measured sphere truncated to 80˚.

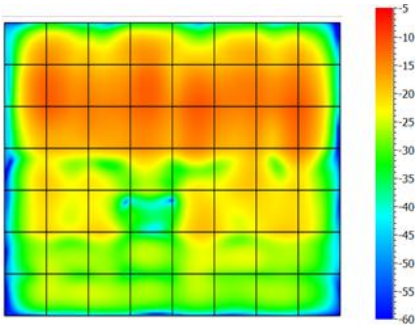

Figure 6 - Amplitude of the *y*-component of the tangential electric field from the 3D reconstruction, with patch size of 0.8 λ, enhanced accuracy and a measured sphere truncated to 60˚.

To study the measurement sampling effect, the SWE of the original measured field was used to compute the field on a full sphere with sampling in theta and phi of 3.6˚. This value corresponds to an oversampling factor of 1.6 relative to the minimum sampling of 5.8˚. This produced 5100 field samples on a full sphere, which allowed one to use again the "enhanced" accuracy and 0.8 λ of patch size. The result of the reconstruction is shown in Figure 7.

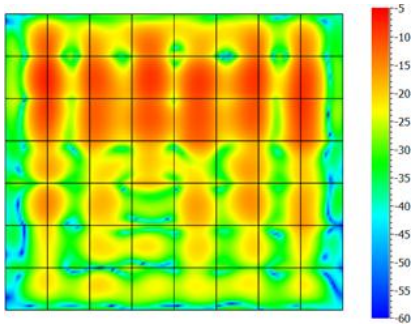

Figure 7 - Amplitude of the *y*-component of the tangential electric field from the 3D reconstruction, with patch size of 0.8 λ, enhanced accuracy, full sphere data, and oversampling of 1.6.

It is seen that all slots are identified and that the result almost coincides with that of Figure 3. As long as full sphere data is available, with a sampling according to Eqs. (5)-(6), the sampling does not play a key role in the reconstruction. The sphere with 3.6˚ sampling was then truncated to 82.8˚, giving rise to 2400 measured points and thus approximately 4800 possible unknowns. To decrease the number of unknowns of the reconstruction, the patch size was kept equal to 0.8 λ while the accuracy was set to "normal", generating 4752 unknowns. The result is shown in Figure 8.

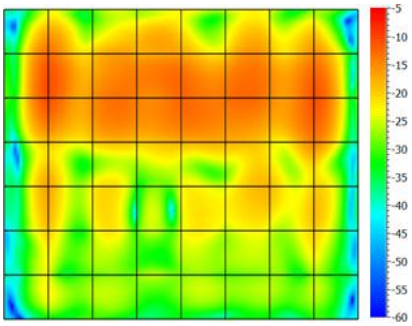

Figure 8 - Amplitude of the *y*-component of the tangential electric field from the 3D reconstruction, with patch size of 0.8 λ, normal accuracy, measured sphere truncated to 82.8˚and oversampling of 1.6.

If we compare it with Figure 4 and Figure 6 we can see that the pictures are very similar. This means that a lower oversampling, combined with a truncated sphere, affects the resolution achievable with the 3D reconstruction, producing results almost equivalent with the traditional microwave holography. This conclusion is also confirmed by the results presented in [11], where the 3D reconstruction achieved the same results as microwave holography, when applied to a slotted waveguide array with measured data truncated to a 80 ˚ sphere and an oversampling factor of 1.6.

4. Conclusions

The 3D reconstruction algorithm was applied to a slotted waveguide array measured at the DTU-ESA Spherical Near-Field Antenna Test Facility. One slot of the array was covered by conductive tape and an error was present in the array excitation. Both defects could successfully be detected, and all slots could be identified. It was shown that the spatial resolution provided by the 3D reconstruction is much higher than that provided by traditional microwave holography, where the individual slots cannot be resolved. This happens when measured full sphere data are available and when the measured field sampling is almost a factor 3 or 1.5 higher the minimum sampling defined by spherical wave theory. It was also illustrated that when the length of the patches describing the reconstruction surface is chosen equal to the spacing of the array elements the accuracy of the reconstructed field increases. Finally it was shown that truncated measurements data affects the accuracy of the reconstructed field. When the measured field is truncated but oversampled by a factor 3 relative to the minimum sampling defined by spherical wave theory, this reduction in accuracy is however limited and the obtained results still allow to roughly identifying the individual slots. However, when the oversampling of the truncated measured field is decreased to around 1.5, slots cannot be resolved and the result almost coincides with that provided by microwave holography.

5. REFERENCES

[1] H. G. Booker, P. C. Clemmow, "The concept of angular spectrum of plane waves and its relation to that of polar diagram and aperture distribution", Proc. Inst. Elec. Eng., vol. 97(1), pp. 11-16, January 1950.

[2] C. Cappellin, O. Breinbjerg, A. Frandsen, "Properties of the transformation from the spherical wave expansion to the plane wave expansion", Radio Science, vol. 43, no. RS1012, doi:10.1029/2007RS003696, February 2008.

[3] T. K. Sarkar, A. Taaghol, "Near-field to near/far-field transformation for arbitrary near-field geometry utilizing and equivalent electric current and MoM," IEEE Trans. Antennas Propagat., vol. 47, no. 3, pp. 566–573, Mar. 1999.

[4] Y. Alvarez, F. Las-Heras, M. R. Pino, "Reconstruction of equivalent currents distribution over arbitrary three-dimensional surfaces based on integral equation algorithms", IEEE Trans. Antennas Propagat., vol. 55, no. 12, pp. 3460–3468, Dec. 2007.

[5] J. L. A. Quijano, G. Vecchi, "Improved-accuracy source reconstruction on arbitrary 3-D surfaces", IEEE Antennas and Wireless Propagation Letters, vol. 8, pp. 1046–1049, 2009.

[6] K. Persson and M. Gustafsson, "Reconstruction of equivalent currents using a near-field data transformation - with radome applications", Progress in Electromagnetics Research, vol. 54, pp. 179–198, 2005.

[7] T. F. Eibert, C. H. Schmidt, "Multilevel fast multipole accelerated inverse equivalent current method employing Rao-Wilton-Glisson discretization of electric and magnetic surface currents", IEEE Trans. on Antennas Propag., vol. 57, no. 4, pp. 1178–1185, 2009.

[8] E. Jørgensen, P. Meincke, C. Cappellin, and M. Sabbadini, "Improved source reconstruction technique for antenna diagnostics", Proc. of the 32nd ESA Antenna Workshop, ESTEC, Noordwijk, The Netherlands, 2010.

[9] E. Jørgensen, P. Meincke, O. Borries, and M. Sabbadini, "Processing of measured fields using advanced inverse method of moments algorithm", Proc. of the 33rd ESA Antenna Workshop, ESTEC, Noordwijk, The Netherlands, 2011.

[10] E. Jørgensen, J. L. Volakis, P. Meincke, and O. Breinbjerg, "Higher order hierarchical Legendre basis functions for electromagnetic modelling", IEEE Trans. Antennas Propagat., vol. 52, no. 11, pp. 2985–2995, Nov. 2004.

[11] E. Jørgensen, D. W. Hess, P. Meincke, O. Borries, C. Cappellin, J. Fordham, "Antenna diagnostics on planar arrays using a 3D source reconstruction technique and spherical near-field measurements", Proc. of EuCAP 2012, Prague, 2012.

[12] F. Jensen, A. Frandsen, "On the number of modes in spherical wave expansions", Proc. Antenna Meas. Tech. Ass. Symposium, AMTA 2004, pp. 489-494, 2004.

[13] J. J. Lee, E. M. Ferren, D. P. Woollen, K. M. Lee, "Near-field probe used as a diagnostic tool to locate defective elements in an array antenna", IEEE Trans. Ant. Prop., vol. 36, no. 6, June 1988.

[14] D. W. Hess, S. T. McBride, "Imaging of element excitations with spherical scanning", Proc. Antenna Meas. Tech. Ass. Symposium, AMTA 2011, pp. 329-334, 2011.